Improved Electrical Performance through Laser Modification of Monolayer Transition Metal Dichalcogenides

HO JIN QING

A0065533H

PC4199 Honours Project in Physics

In Partial Fulfilment of the Requirements for the Degree of Bachelor of Science (Honours)

Department of Physics

National University of Singapore

AY2014/2015

Table of Contents

List of Figures

List of Tables

Acknowledgements

This FYP journey has been an enriching and meaningful experience. It is a blessing to be able to continue my research experience in the Nanomaterials Research Lab after completing my UROPS project in Year 3 Semester 1. This cherished experience would not have been possible without the help and support that I have received.

Firstly, I would like to extend my utmost gratitude to Prof Sow Chorng Haur, who offered me the opportunity to do a UROPS project in his laboratory when I was in Year 3, and saving a place for me as his FYP student when I went on student exchange. I am really thankful for his kind and patient guidance, especially at the initial phase when I was clueless at the beginning of my UROPS. His passion in both research and teaching has inspired me greatly. His emphasis on interpersonal relationships and a friendly work environment has also inculcated a lab culture that is very loving and comfortable to learn and work in. I enjoyed the lab meetings we have, as we get a chance to update one another about our progress, interact and know more about each other at a more personal level, and feel like we are one big family.

Secondly, I would like to thank my helpful and friendly mentor, Dr Lu Jun Peng. Since my UROPS days, he has provided me with a lot of help and support, explaining concepts and providing valuable advice. I am extremely grateful to have him as my mentor and I am glad to know him at a more personal level instead of just having a work relationship.

I would also like to thank everyone in the Nanomaterials Research lab for guiding and supporting me in one way or another. I am especially grateful to Mr Zheng Minrui, Dr Lim Xiaodai Sharon, Mr Lim Kim Yong, Mr Chen Gin Seng and Miss Gong Lili for their guidance and advice, as well as my fellow FYP friends, Ang Jian Martin and Kwang Siu Yi, for the fun and laughter, frustration and stress that we shared. I really enjoyed my one and a half years in this lab.

Not forgetting the many other people who have walked me through my FYP days, I want to thank my family for being understanding and supporting me during the stressful period of my final year in NUS. I am also very thankful for the friends who have accompanied me through this period, especially my VCF (Varsity Christian

Fellowship) friends. It was definitely more enjoyable and meaningful to be able to share the journey with loving and supportive friends.

Last but not least, I thank God for this opportunity to learn and grow in my final year in NUS, to be able to gain research experience through my FYP. He has blessed me with helpful and kind people in the lab, caring and supportive friends in my life, wisdom and strength in handling my different commitments in Year 4, and also challenges to grow and mature me.

Abstract

Monolayer transition metal dichalcogenides (TMDs) have attracted much attention recently due to their potential in the new generation of optoelectronic and nanoelectronic devices. Thus, the synthesis and characterization of these two-dimensional (2D) monolayer materials, as well as device fabrication with TMDs have been of considerable interest. Particularly, these 2D materials have attractive physical and chemical properties in their monolayer form, such as the property of having a direct band gap, which makes them good candidates for efficient light emission as compared to their bulk counterparts, allowing for applications in devices such as transistors, photodetectors and electroluminescent devices, just to name a few.

In this work, the growth of WSe_2 and MoS_2 monolayer flakes using a chemical deposition (CVD) method in a horizontal tube furnace is reported. The CVD method used involves Se/S powder and WO_3/MoO_3 powder as precursors with a constant flow of gas. It is based on a simple chemical process, synthesizing WSe_2 and MoS_2 directly on sapphire or Si/SiO_2 substrates. The growth parameters are successfully optimized for the synthesis of both WSe_2 and MoS_2 monolayer flakes and islands. Following that, the properties of these monolayer TMDs were analyzed and characterized. Thereafter, various devices, such as the Field Effect Transistor (FET) devices, are then fabricated based on these monolayer TMD flakes and islands to investigate their electrical properties. It is found that the ion gel FET devices fabricated from WSe_2 monolayer islands can exhibit a carrier mobility of 0.0541 cm^2/Vs for the hole transport, an on/off ratio of approximately $2.54x10^3$ and a carrier concentration of $8.7x10^{15}$ cm^{-3}.

With the aim of improving the electrical properties of the monolayer TMDs, the effects of a focused laser beam irradiation as a post-synthesis step is experimented with in this project. It has been found that upon laser modification, WSe_2 exhibits increased electronic response, as seen in the increase in carrier mobility from 0.0541 cm^2/Vs to 0.405 cm^2/Vs upon laser beam modification. Also, the on/off ratio maintained at a magnitude of 10^3.

The results obtained thus far present a promising method to enhance TMD materials for the fabrication of devices with excellent characteristics.

1. Introduction

Substantial research has been done with graphene, a 2D material found to have great electrical, mechanical and optical properties[1-3]. However, due to its absence of a band gap, field effect transistors (FETs) fabricated from graphene have high off-currents[4,5]. Hence, interest in monolayer transition metal dichalcogenides (TMDs), which have direct band gaps, has been growing, as they hold great potential in the new generation of optoelectronic and nanoelectronic devices[6-8]. In recent years, much research has been done in the synthesis, characterization and application of these two-dimensional (2D) monolayer materials[6-10].

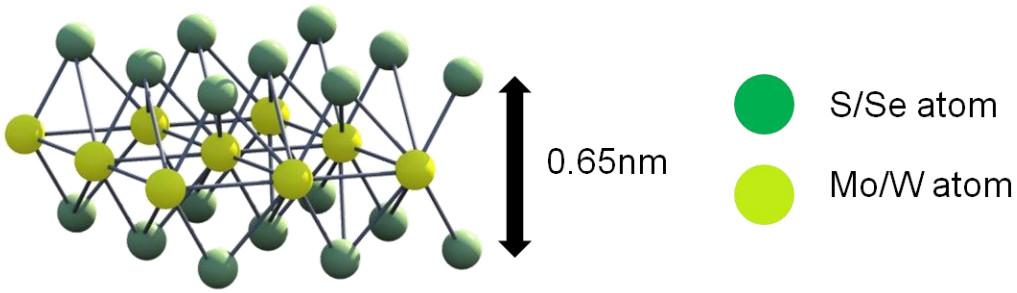

Figure 1. Structure of monolayer TMDs.

TMDs (MX_2, M=Mo, W, X=S, Se) are formed by a layer of transition metal atoms between two layers of chalcogen atoms. A monolayer TMD is approximately 6.5Å in thickness[11]. Within the layers of TMDs, the interlayer atoms are bonded by strong covalent bonding, but a weak van der Waals bonding exist between the layers[12,13]. Monolayer TMDs have direct band gaps, which make them good candidates for efficient light emission as compared to their bulk counterparts, as well as potential discoveries of promising electronic properties. From literature, the direct band gaps of monolayer WSe_2, WS_2, MoS_2 and $MoSe_2$ are 1.65eV[14], 1.93eV[15], 1.84eV[16] and 1.55eV[17] respectively. The presence of direct band gaps allows for applications such as transistors, photodetectors and electroluminescent devices[6-8].

2. Background

2.1 Synthesis

2.1.1 Chemical Vapor Deposition

A common method used to synthesize monolayer TMDs is the scotch-tape based micromechanical cleavage method, one of the top-down exfoliation methods, to exfoliate single-layer TMDs[6,11]. However, this method has various limitations, such as the lack of control over the flake thickness and size, which is likely to be crucial for nanoelectronics and optoelectronics[6].

Another widely explored method in the recent years is the chemical vapor deposition (CVD) method, a bottom-up approach. The existing CVD methods vary; each uses different solid precursors heated to a high temperature. For example, one method uses sulphur powder and MoO_3 powder vaporized and co-deposited onto a nearby substrate[6], another directly uses WSe_2 powder placed in an alumina boat with growth substrates placed at the downstream end for deposition[18], and yet another involves the deposition of a thin layer of Mo metal onto a wafer heated with solid sulphur[6]. These CVD methods are able to synthesize reasonably good quality material with typical flake sizes of hundreds of nanometers to a few micrometers[6]. It has also been reported that monolayer WSe_2 synthesized with the CVD approach demonstrated excellent crystalline quality and that p-type WSe_2 field-effect transistors (FETs) fabricated from monolayer WSe_2 exhibit great electronic characteristics[18]. Therefore, the synthesis of monolayer TMDs by chemical vapor deposition is of interest in this project.

2.1.2 Seeding Promoters

On top of the promising synthesis of monolayer TMDs using the CVD method, there has also been research exploring the usage of seeding promoters to achieve high-quality and uniform monolayer TMDs[19-21].

Seeding promoters are aromatic molecules such as perylene-3,4,9,10-tetracarboxylic acid tetrapotassium salt (PTAS), 3,4,9,10-perylene-tetracarboxylicacid-dianhydride (PTCDA) and reduced graphene oxide (r-GO)[19,21]. They have high thermal stability and assist to gain better control of the synthesis of

high quality monolayer TMDs. They act as the preferential nucleation sites for the growth of monolayer TMDs, hence behaving like a catalyst of the synthesis process. In previous research done, it was found that substrates can be treated with either a drop of rGO-hydrazine solution, PTAS (50μm) or PTCDA (26mg in 5mL DI water) solution[21].

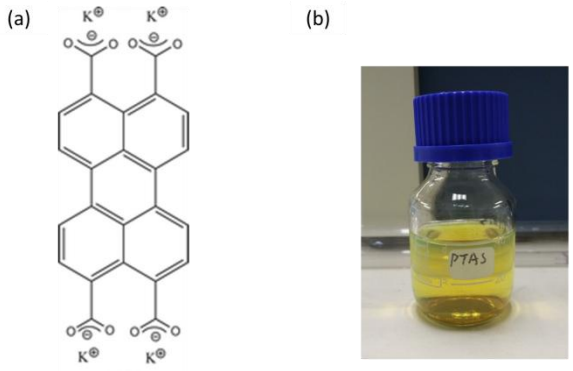

Figure 2. (a) Structure of PTAS. (b) Picture of PTAS solution.

In particular, PTAS has been found to be able to withstand a higher temperature than other seeding promoters. It demonstrates good thermal stability and a slow decomposition rate when the growth temperature is below 820^{o}C [20]. Figure 2 shows the chemical formula of PTAS and a picture of the PTAS solution.

2.2 Focused Laser Beam Modification

The ability to synthesize uniform monolayer TMDs is greatly looked into and required in the applications of TMDs in recent years. The application and good performance of single-layer WSe_2 and MoS_2 transistors have been reported separately[8,11,22]. The difficulty of maintaining consistency in the synthesis of single layer TMDs is commonly faced due to a lack of control of the thickness. Even in the CVD method used in this project, it is found that slight variations of pressure, temperature and growth time during the growth process lead to different thickness of the TMDs grown. There is also limited control over the uniformity of the TMDs. Recently, there has been research done in using a focused laser spot to thin MoS_2 down to monolayer thickness by thermal ablation[23]. It is reported that the process relies on the sublimation of the upper layers of MoS_2 due to heating induced by the absorption of laser light. As the bottom layer is in intimate contact with the substrate which acts as a heat sink, it will remain on the substrate until a much higher laser power is used[23].

Previously, it has also been reported that by using a unique focused laser beam setup that birthed from recent innovative studies conducted by some members of our Nanomaterials Research Lab, properties of nanomaterials can be modified for effective photonic and optoelectronic applications. It was found that the electrical conductivity of the modified MoS_2 material increased by more than ten times, while the photoconductivity increased by about five times[24]. This unique technique has also successfully modified the chemical composition of the ternary compound CdS_xSe_{1-x} nanobelts when they were subjected to a treatment of focused laser beam destruction[25]. In doing so, the photoluminescence properties of the nanobelts are controlled and changed.

This presented many possibilities of material modification and new findings by subjecting synthesized TMDs to a focused laser beam with this unique setup in our lab. Therefore, in this project, the effect of laser modification of TMDs on their electrical properties is investigated.

2.3 Field Effect Transistors (FETs)

A transistor in general is a device with three terminals where the channel resistance between two of the contacts is controlled by the third contact. Field effect transistors (FET) are voltage controlled devices which behave such that the channel is controlled by an external electric field, hence the name field effect. Conventionally, the channel carriers flow from the source to the drain, and the control terminal, also known as the gate terminal, provides the electric field that controls the channel resistance[26]. A schematic diagram of an FET is shown in Figure 3a.

FETs have many attractive applications, such as to switch or amplify electronic signals, which has practical uses in electronics like hearing aids and computer chips[27]. A family tree of FETs is shown in Figure 3b. The three first-level main members are the insulated-gate FET (IGFET), junction FET (JFET) and metal-semiconductor FET (MESFET), which are distinguished by the method of formation of the gate electrode. The gate electrode is an insulator, a depletion layer of a p-n junction and a Schottky barrier for the three different categories respectively. In the branch of IGFET, we further divide it into metal-insulator-semiconductor FET (MOSFET/MISFET), where MOSFET's insulator is specifically a grown oxide layer and MISFET's insulator is a deposited dielectric, and heterojunction FET (HFET). In

the HFET branch, the material of the gate electrode is a high band gap semiconductor layer grown as a heterojunction which acts as an insulator.

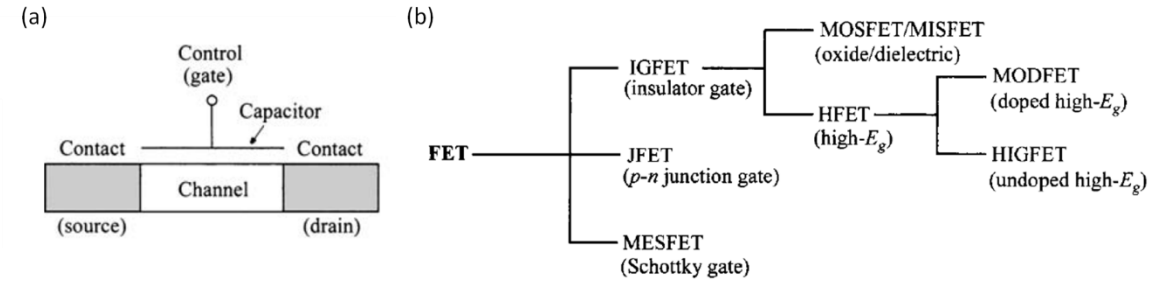

Figure 3. (a) Schematic diagram of a typical FET[26]. (b) Family tree of FETs[26].

In the basic FET structure, which has been adapted to 2D TMDs, a semiconducting channel region is connected to the source and drain electrodes, and separated by a dielectric layer from a gate electrode. The current flowing between the source and drain electrodes is controlled by the gate electrode which modulates the conductivity of the channel. A voltage drop across the dielectric layer caused by the gate electrode induces a conducting channel between the source and drain contacts via field effect[6]. In a semiconductor, the lower density of electrons or holes that can respond to an applied field is sufficiently small, therefore, the field can penetrate quite far into the material[28]. With an increase in the dielectric field which adds carriers to the channel, the conductivity of the channel increases[28]. The first implementation of a top-gated transistor based on monolayer MoS_2 was reported to show excellent on/off current ratio of 10^8, n-type conduction and a decent room-temperature mobility of >200cm^2/Vs[6].

The most commonly used dielectric is SiO_2, but in this project, a special class of solid polymer electrolytes known as ion gels are used. Ion gels are prepared from mixtures of an ionic liquid and a block copolymer[29]. As ionic liquids are moisture sensitive, solution preparation and electrical measurements have to be carried out in a glovebox[29]. They can be used as gate insulators for FETs, and have been seen to create dramatic improvements in conductivity which allow for lower voltages applied, higher currents generated and higher durability[28]. It has been demonstrated before that ion gels have very large concentration and mobility of ionic species[30], which spell substantial promise for improvements in performance of electronics that requires gate dielectrics.

3. Experimental Methodology

3.1 Chemical Vapor Deposition

The CVD method has been repeatedly reported to be able to synthesize highly crystalline and good quality TMDs[9,18] and is a low-cost approach to directly grow TMDs on SiO_2[7]. It is used to synthesize the TMDs used in our experiments. Powder is typically used as precursors and is vaporized at high temperatures. In this project, two different setups are used for the synthesis process.

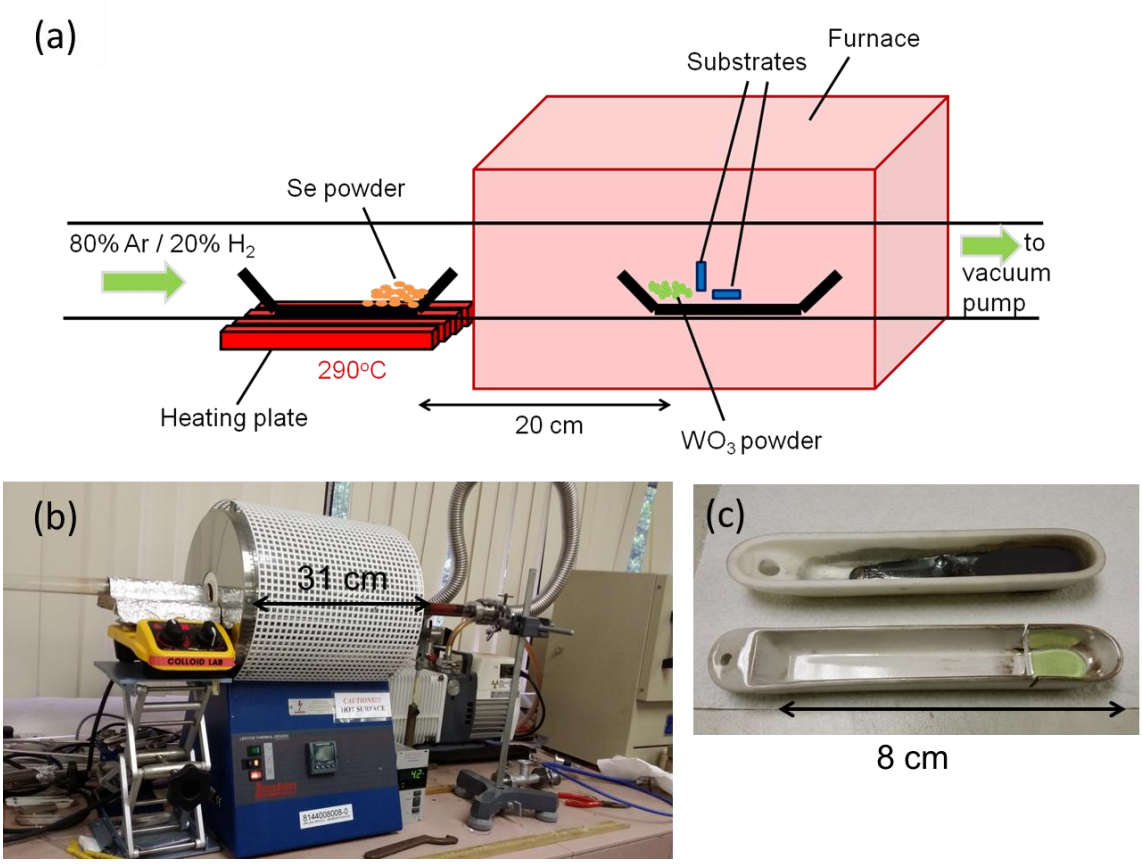

Figure 4. (a) Schematic diagram of the first setup and pictures of (b) tube furnace used to synthesize WSe_2 and (c) crucibles with sapphire substrates and WO_3 powder, and with selenium powder.

The first setup, which is used for the synthesis of WSe_2 in this project, is as shown in Figure 4. The substrates, which are sapphire substrates, were placed upright and horizontally downstream, beside the WO_3 powder in a ceramic crucible, such that the polished surface faces the powder. The WO_3 crucible is then placed in a 2.54 cm diameter quartz tube, at the centre of the horizontal furnace (Lenton Thermal

Designs, LTF 12/38/250), and another ceramic crucible that contains selenium powder is placed 20 cm upstream from the WO_3 crucible. The Se crucible is positioned outside the furnace, such that it is directly above a hot plate, which can control the temperature that the Se powder is to be heated to. Gas (80% Argon, 20% Hydrogen) is introduced into the tube from one end, controlled by a mass flow controller, and the other end can either be connected to the atmosphere outside the lab or to a vacuum pump, which can create a lower pressure in the tube and allow for better control of the pressure. Under a continuous gas flow, the temperature of the furnace is set to increase gradually from room temperature to the reaction temperature at a specified rate. The hot plate is manually switched on and kept at 290^{o}C when the furnace reaches a certain temperature. Upon reaching the reaction temperature, the furnace is kept at this reaction temperature for a specific period of time and allowed to cool down to room temperature naturally thereafter.

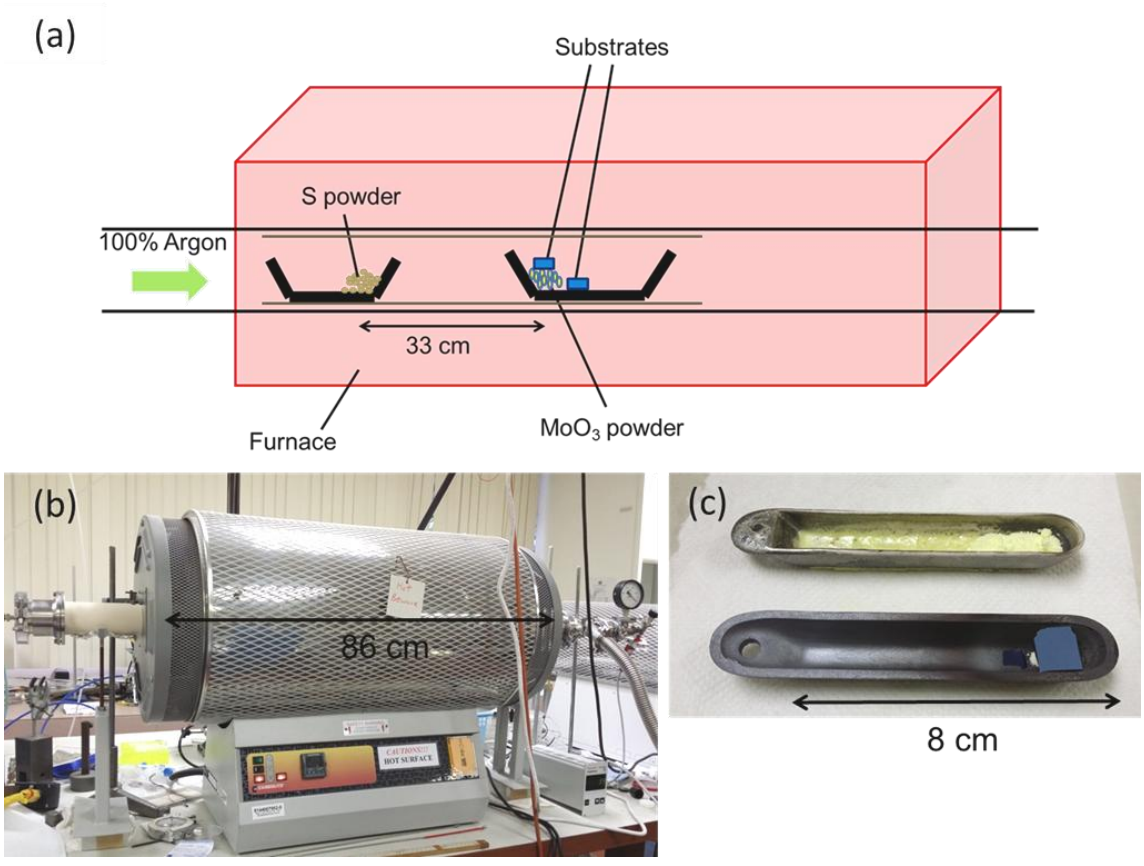

Figure 5. (a) Schematic diagram of the second setup and pictures of (b) tube furnace used to synthesize MoS_2 and (c) crucibles with Si/SiO_2 substrates and MoO_3 powder, and with sulphur powder.

The second setup, which is used to synthesize MoS_2 in this project, is as shown in Figure 5. One sample is placed face-down above the MoO_3 powder without touching it, while the other is placed face-up downstream beside the powder in a ceramic crucible, as shown in Figure 5c. The MoO_3 crucible is placed in a 2.4 cm diameter quartz tube, at the centre of a big horizontal tube furnace (Carbolite, STF 15/450), and another ceramic crucible that contains sulphur powder is placed 33cm upstream from the MoO_3 crucible. Gas (100% Argon) is introduced into the tube from one end, controlled by a mass flow controller, and the other end of the tube can either be connected to the atmosphere outside the lab or to a vacuum pump. Under a continuous gas flow, the temperature of the furnace is set to increase gradually from room temperature to the reaction temperature at a specified rate, and upon reaching this temperature, the furnace is kept at it for a specific period of time. The furnace is then allowed to cool down to room temperature naturally.

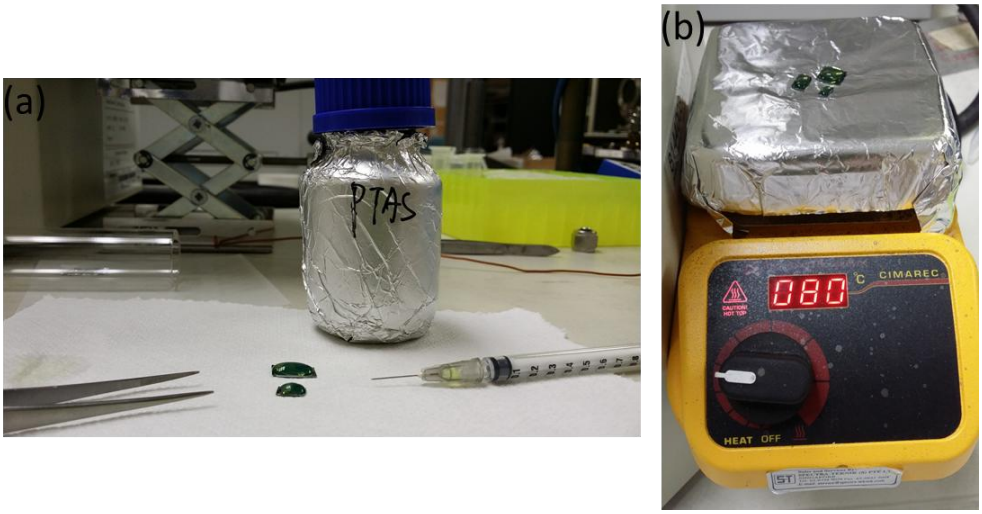

Figure 6. Pictures of (a) the addition of PTAS to Si/SiO_2 substrates and (b) Si/SiO_2 substrates on a heating plate set to 80^oC.

The effectiveness of seeding promoters promoting monolayer growth is explored and found to be possible with a slight variation of the second setup. Instead of using a tube opened at both ends, a 2.4 cm diameter quartz tube closed at one end is used. PTAS (50μm) is added drop-wise on the substrates until the surface of the substrates are fully covered by PTAS, as shown in Figure 6a. The substrates are then placed on a hot plate kept at 80^oC (Figure 6b) to allow the PTAS to be heated dry. After being treated with PTAS, the substrates are placed in the MoO_3 crucible as

mentioned earlier. Similarly, the MoO_3 crucible is placed at the centre of the big tube furnace, and the sulphur crucible is placed 33cm upstream from the MoO_3 crucible. The subsequent synthesis steps are similar to that stated in the earlier paragraph.

The optimized growth parameters used in this project will be specified and further elaborated in the next section on 'Experimental Results and Discussion'.

3.2 Characterization and Analysis

Various equipments are used for the purpose of analysis and characterization of the synthesized TMDs. The Fluorescence Microscope is used to examine the optical properties of the laser-modified samples by irradiating the samples with lights of different wavelengths, and the Atomic Force Microscope (AFM, Dimension 3100) is used to examine the changes in morphology and identify the thickness of the synthesized TMDs. Photoluminescence (PL) Spectroscopy (Reinshaw InVia system 2000, 532nm) is used to obtain the PL spectra of the various regions of interest, in order to understand the PL properties of the samples. Raman spectroscopy (Reinshaw InVia sytem 2000 micro-Raman machine) is used to test for the presence of the TMDs grown, based on the inelastic scattering of photons when they interact with the phonons in the TMDs.

3.3 Focused Laser Beam Technique

The process of laser modification is conducted using an optical microscope-focused laser beam setup, as shown in Figure 7. A 532 nm laser source is used, whereby the power of the focused laser beam can be varied. A power meter is used to measure the power of the laser beam with precision. The sample is placed on an X-Y motorized stage which is controlled by the computer. This allows precise measurements to be made when creating patterns on the samples using the laser beam. The sample is mounted in a vacuum chamber, which is connected to a vacuum pump, allowing for the option of inducing a vacuum condition to the laser modification process if necessary. To study the effects of laser modification on TMDs, an incident laser power of about 100mW is used to scan across monolayer WSe_2 flakes.

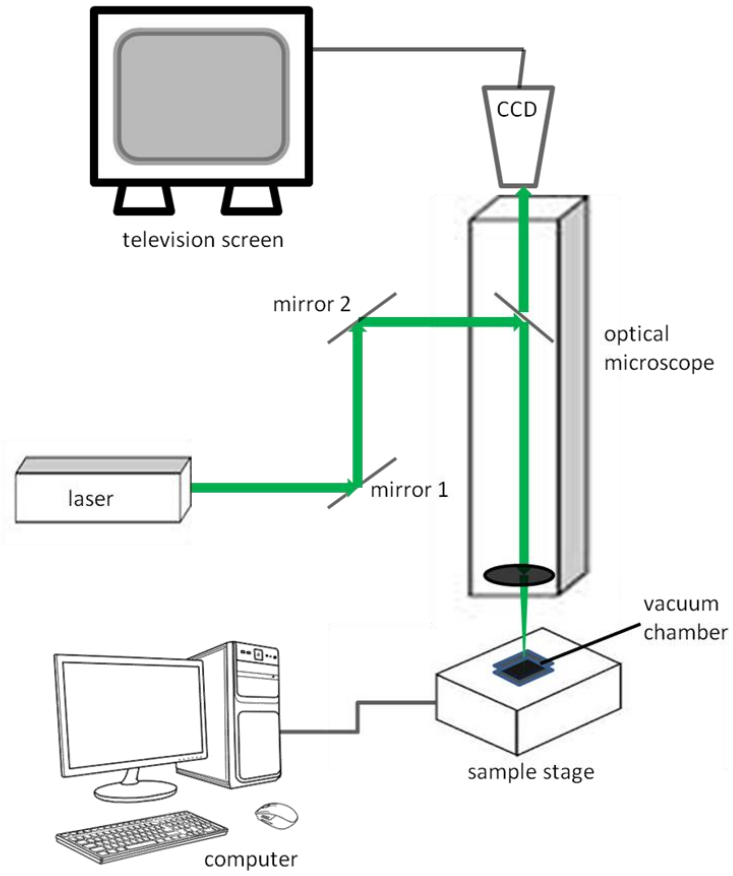

Figure 7. Schematic diagram of the optical microscope-focused laser beam setup.

3.4 Fabrication of Devices

For the fabrication of devices, lithography was done using the Electron Beam Lithography (EBL) technique, using poly(methyl methacrylate) (PMMA) as the photoresist. Electrodes are thermally deposited onto the surface of the TMD, and are positioned such that at least one monolayer TMD flake fall between the electrodes. Pd/Au electrodes are used for WSe_2 devices and Cr/Au electrodes are used for devices fabricated from other TMDs. A schematic diagram of a simple fabricated device are as shown in Figure 8a. Figure 8b shows an optical image of a few simple devices which consist of four electrodes deposited on one monolayer TMD flake.

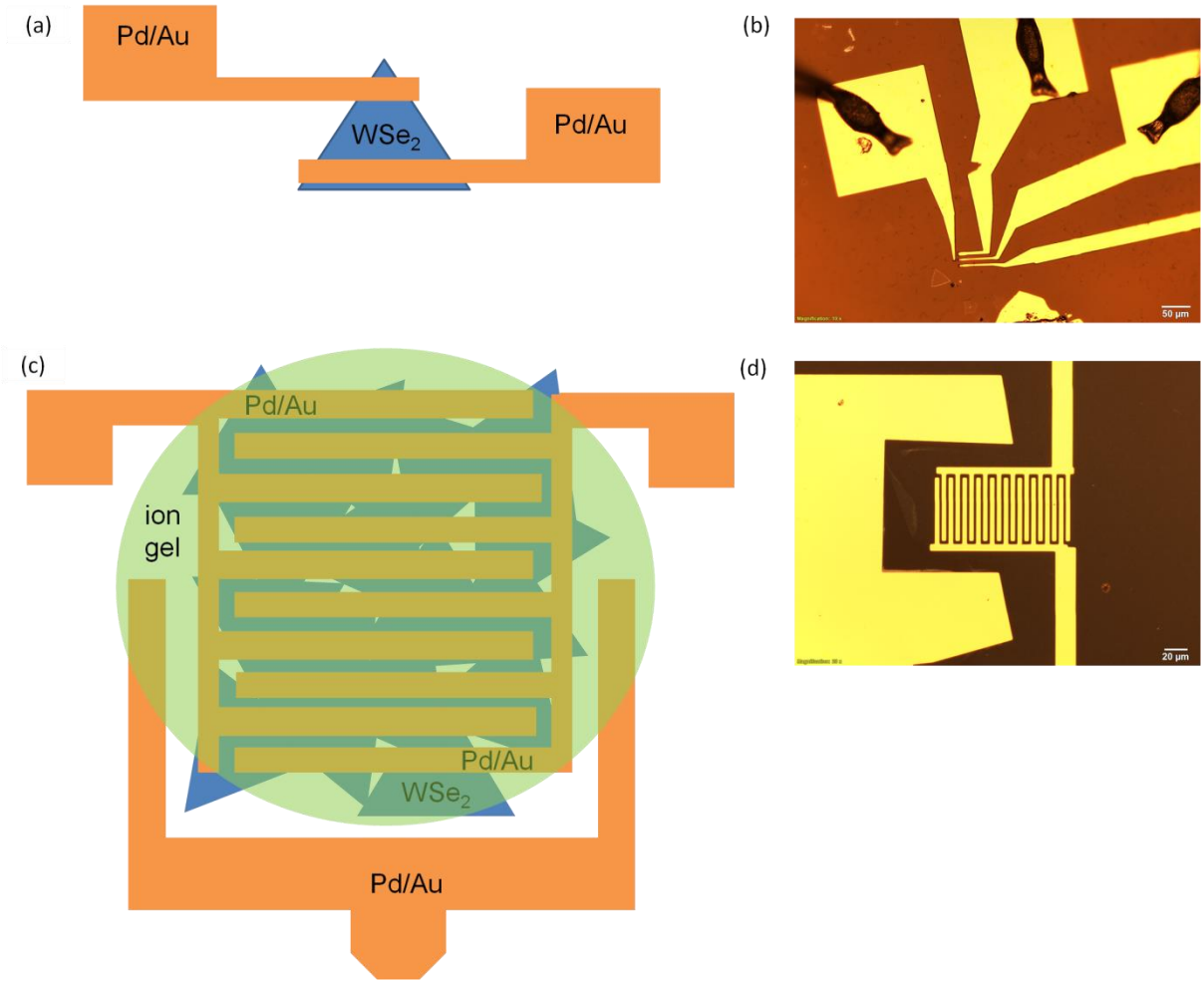

Figure 8. (a) Schematic diagram and (b) optical image of simple devices. (c) Schematic diagram and (d) optical image of ion gel FET devices.

FET devices based on ion gel gating, which is the focus of this project, are synthesized similarly, but with a more complicated architecture as shown in Figure 8c. The source and drain electrodes are designed such that they consist of a number of pins, and they are deposited on an island of monolayer TMD. The gate electrode is deposited beside the island of monolayer TMD. The ion gel solution, a mixture of the polymer, poly (styrene-block-methyl methacrylate-block-styrene) (PS-PMMA-PS), and an ionic liquid, EMIM-TSFI, in an ethyl propionate solvent, is drop-casted above the region of monolayer TMD of interest and used as the side gate dielectrics[31]. Hence, a side-gated FET device based on ion gel gating is fabricated. The device can be wire-bonded to be tested. A schematic diagram of an example of the fabricated ion gel FETs is as shown in Figure 8c and an optical image of another one of them is shown in Figure 8d. The devices fabricated in this project have channel

lengths of 2 or 5 μm and channel widths of 150 μm, and the thickness of the channel material is usually about 0.65 nm, the thickness of monolayer TMDs.

Due to some problems faced with the thermal deposition of electrodes on Si/SiO_2 substrates, the top-gated FETs fabricated with monolayer MoS_2 on Si/SiO_2 substrates could not be used for further analysis in this project.

3.5 I_d-V_d and I_d-V_g measurements

With the fabricated devices, standard transistor measurements are conducted under ambient conditions to find the carrier mobilities, on/off ratios and carrier concentrations of the channel material.

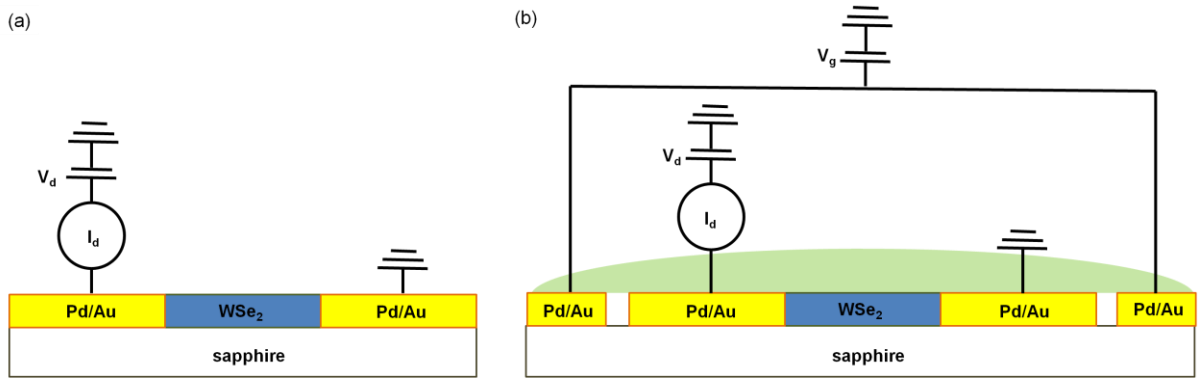

Figure 9. Schematic diagram of electrical connections of a (a) simple device and (b) ion gel FET device.

Figure 9a shows the electrical connections of the simple device, which is connected to a sourcemeter (B2912A Precision Source/Measure Unit). The sourcemeter provides a sweeping DC bias voltage V_d and is able to measure the current flow I_d. Figure 9b shows the electrical connections of the ion gel FET device, which is also connected to a sourcemeter for measurement purposes. For the FET device, there are three terminals instead of two, as the introduction of a gate electrode allows for a gate voltage V_g to be applied to the channel material, thus controlling the conductivity of and hence the current flow in the channel.

The electronic properties of the FET device are determined by measuring the current passing through the electrodes when different drain voltages V_d and gate voltages V_g are used. I_d-V_d graphs are obtained by measuring the current passing through the electrodes when the drain voltage is varied, while applying a constant gate voltage.

I_d-V_g graphs are obtained by measuring the current passing through the electrodes with a varying range of gate voltage, while setting the drain voltage to be constant. The measurements are made under ambient conditions at room temperature.

4. Experimental Results and Discussion

4.1 Synthesis of WSe_2 and MoS_2

Through systematic studies, optimization of growth parameters was carried out and distinguishable monolayer TMDs, typically in triangular-shaped domains, were successfully synthesized, as shown in Figure 10. The size, morphology and quality of the growth can be affected by various factors. The different factors that can be controlled and varied are the type of gas, gas flow, pressure, reaction temperature, ramping speed, growth time and the addition of PTAS, the seeding promoter used in this project.

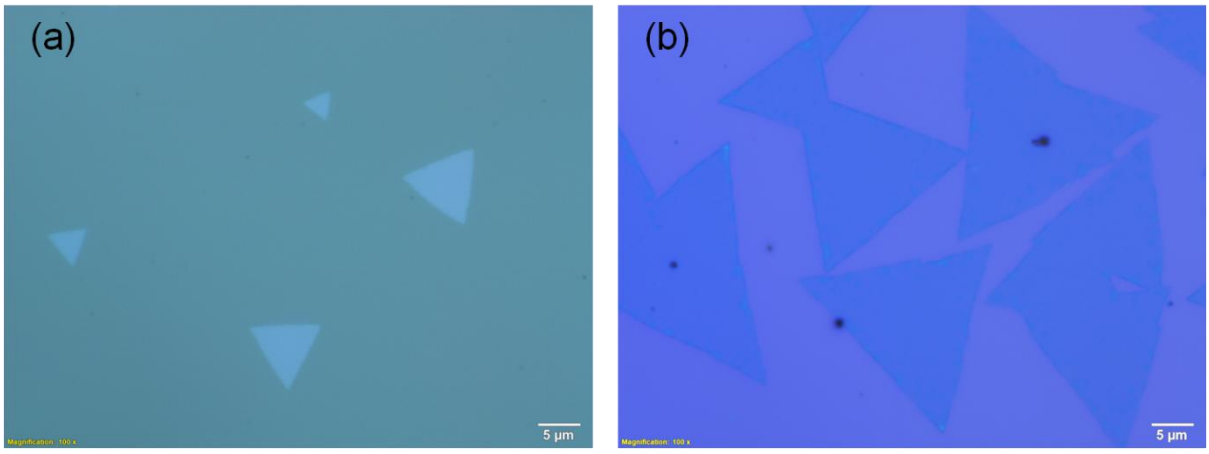

Figure 10. Optical images of successfully synthesized (a) monolayer WSe_2 flakes on sapphire substrate and (b) monolayer MoS_2 flakes on Si/SiO_2 substrate.

The chemical reaction that governs the CVD process of the synthesis of WSe_2 is described as

$$WO_3\,(s) + 3\,Se\,(s) + H_2\,(g) \rightarrow WSe_2\,(s) + H_2O\,(g) + 3\,SeO_2\,(g) \qquad (1)$$

The presence of hydrogen gas is imperative for the selenization of WO_3, as the reaction cannot occur without a reducer due to the low chemical reactivity of selenium[22]. Thus, the gas used for the synthesis of WSe_2 constitutes 80% Argon and 20% Hydrogen.

On the other hand, sulphur, which is above selenium in the periodic table, has a higher chemical reactivity due to higher electronegativity, since its valence electrons are more attracted to the nucleus. Thus, the introduction of a reducer in the reaction

atmosphere is not necessary. Hence, the gas used for the synthesis of MoS_2 is 99% Argon. The chemical reaction is described as

$$2\ MoO_3\ (s) + 7\ S\ (s) \rightarrow MoS_2\ (s) + 3\ SO_2\ (g) \qquad (2)$$

Slight variations in pressure have been found to greatly affect the growth of monolayer TMDs. For the synthesis of WSe_2, through numerous attempts to optimize the growth parameters, it is experimentally observed that if the pressure is too low, the monolayer flakes will generally be smaller in size; an optical image of this is shown in Figure 11d. On the other hand, if the pressure is too high, either multi-layer flakes will be formed or the flakes will be too densely distributed on the substrate, thus forming a continuous film, as shown in Figure 11a and Figure 11b. However, it is also observed that during each run of the CVD process, the growth of WSe_2 on the sapphire substrates are usually not entirely uniform throughout the substrate. Thus, the growth on one piece of substrate may vary, like Figure 11c, where monolayer and multi-layer WSe_2 are both present. This is especially so for the substrate that is placed horizontally downstream; this is likely due to the varying distance of different positions on the substrate from the precursors. Currently, the ideal pressure for reaction has been concluded to be 4.2 Torr, which is the pressure that is consistently able to synthesize WSe_2 flakes and islands that are largely monolayer.

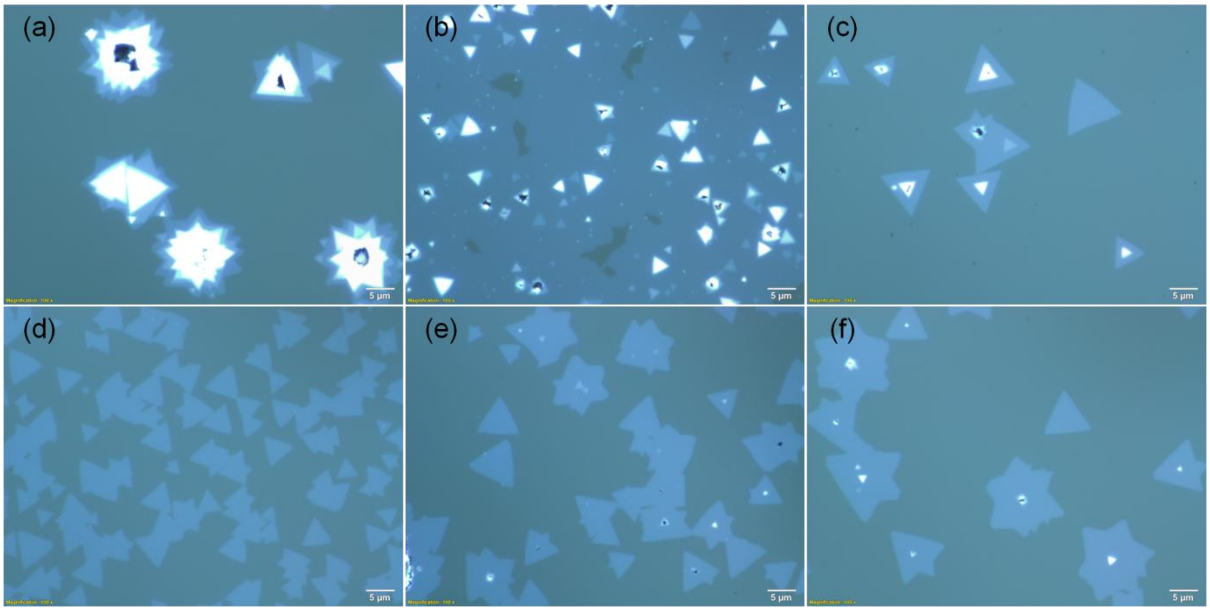

Figure 11. Optical images of WSe_2 on sapphire, synthesized during different runs of the CVD process.

Another interesting factor that is varied is the addition of a seeding promoter, PTAS. Two separate sets of parameters have been found for the synthesis of MoS_2, one involving the pre-synthesis step of introducing PTAS to the substrate and the other without. It has been found that monolayer MoS_2 synthesized using the method that involves the addition of PTAS has a more uniform morphology. This will be further elaborated on in the next sub-section on 'Characterization of WSe_2 and MoS_2'. However, further studies need to be conducted to achieve better control over the amount of PTAS used. The current method of drop-casting the PTAS on the substrates and heating dry on a hot plate kept at 80^oC has little control over the concentration of the PTAS molecules, which is hypothesized to greatly influence the growth result. Each time the PTAS is heated dry, the patterns left on the substrate differs. Also, it is observed that monolayer MoS_2 flakes can grow at regions away from the PTAS patterns left on the substrates after the pre-synthesis treatment, and the PTAS-patterned areas tend to grow MoS_2 particles of greater thickness. An example of this is shown in Figure 12.

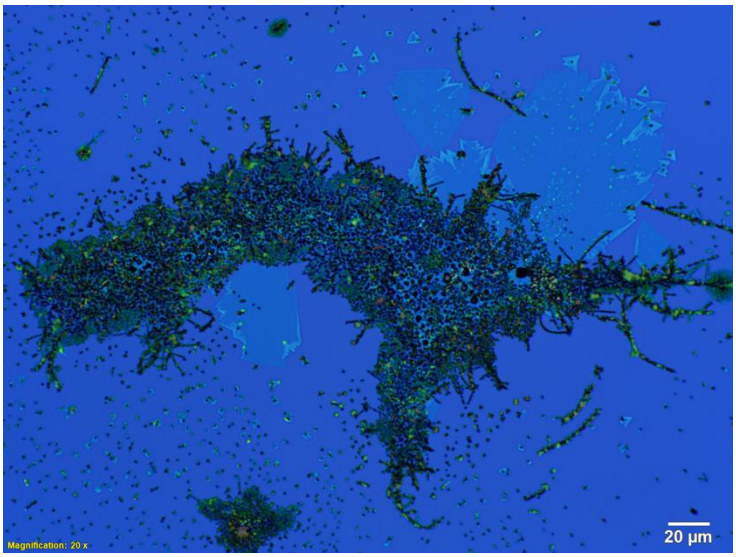

Figure 12. Optical image of a MoS_2 sample with visible PTAS patterns.

Hence, better control over the concentration of PTAS on the substrates will allow the optimum PTAS concentration to be found, which is important for the growth of monolayer MoS_2. This can be explored by placing a separate promoter substrate covered with condensed PTAS, which is left to dry naturally after being drop-casted, upstream of the growth substrate[19]. The concentration of PTAS is predicted to decrease with the distance from the promoter substrate. While optimizing the PTAS

concentration for the best growth of monolayer MoS_2, the reduction of the undesired growth of MoS_2 particles could possibly be achieved with this method too.

As for the gas flow, reaction temperature, ramping speed and growth time, they are largely experimented with and modified from the parameters obtained through various literature. A summary of the successfully optimized parameters are as shown in Table 1.

TMD	**Substrate**	**Gas Flow (sccm)**	**Pressure (Torr)**	**Reaction Temperature (^oC)**	**Ramping Speed (^oC/min)**	**Growth Time (min)**
WSe_2	sapphire	100	4.2	950	28	15
MoS_2	Si/SiO_2	10	atmospheric	600	15	5
MoS_2	Si/SiO_2 treated with PTAS	50	atmospheric	750	28	15

Table 1. Table of optimized parameters for the synthesis of WSe_2 and MoS_2.

For the growth of WSe_2, a gas flow of 100 sccm (80% Argon, 20% Hydrogen) is introduced into the tube from one end and the pressure in the furnace is adjusted to 3.7 Torr by controlling the vacuum pump connected at the other end of the tube. Under the continuous gas flow, the temperature of the furnace is gradually increased from room temperature to 950^{o}C at a rate of 28^{o}C/min. When the temperature within the furnace reaches 770^{o}C, the hot plate is switched on and kept at 290^{o}C, while the pressure is adjusted to 4.2 Torr. When the furnace reaches the highest temperature of 950^{o}C, it is kept at this reaction temperature for 15 minutes and is allowed to naturally cool down to room temperature thereafter.

For the growth of MoS_2 without the usage of PTAS, a gas flow of 500 sccm (100% Argon) is first introduced into the tube from one end and the other end of the tube is connected to the atmosphere. The temperature of the furnace is gradually increased from room temperature to 105^{o}C at a rate of 40^{o}C/min, and set to maintain at this temperature for 30 minutes. Following that, the gas flow is lowered to 10 sccm and the temperature of the furnace is increased to 600^{o}C at a rate of 15^{o}C/min, and it is

kept at this reaction temperature for 5 minutes. The furnace is then allowed to cool down to room temperature naturally.

For the growth of MoS_2 with the usage of PTAS, a continuous gas flow of 50 sccm (100% Argon) is used, and the temperature of the furnace is gradually increased from room temperature to 750^{o}C at a rate of 28^{o}C/min. The furnace is kept at the reaction temperature of 750^{o}C for 15 minutes and is allowed to naturally cool down to room temperature thereafter.

4.2 Characterization of WSe_2 and MoS_2

4.2.1 Raman Spectroscopy

To investigate the lattice structural property of the synthesized WSe_2 and MoS_2, Raman spectroscopy was carried out. Raman spectra for the as-grown monolayer WSe_2 and MoS_2 excited by a 532 nm laser are shown in Figure 13.

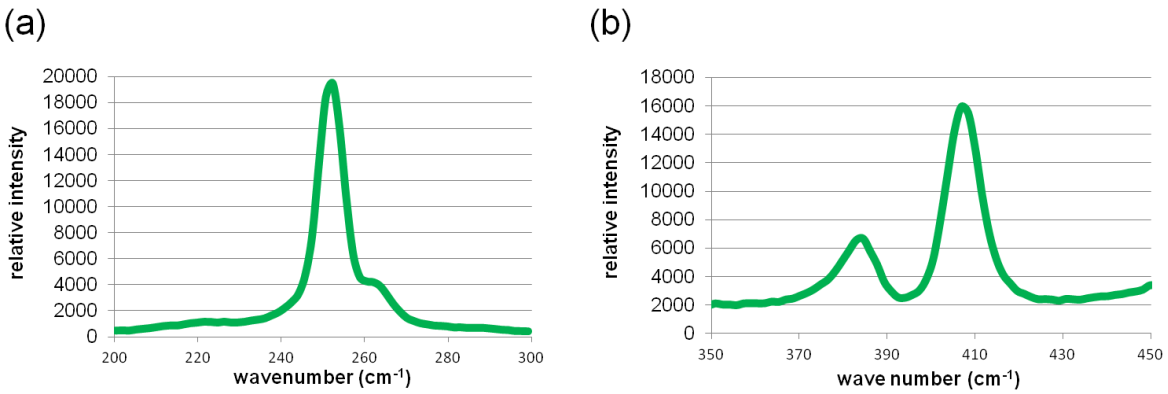

Figure 13. Raman spectra of as-grown monolayer (a) WSe_2 and (b) MoS_2.

The two characteristic peaks for monolayer WSe_2 at 252 cm^{-1}, which corresponds to the in-plane E^1_{2g} mode, and 261 cm^{-1}, which corresponds to its out-of-plane A_{1g} mode, are observed[22,32]. These are two out of the four Raman active modes of WSe_2; the E^2_{2g} mode is found at very low frequencies of approximately 30cm^{-1} and the E_{1g} mode is forbidden in back-scattering geometry on a basal plane[33]. These Raman modes are shown in Figure 14.

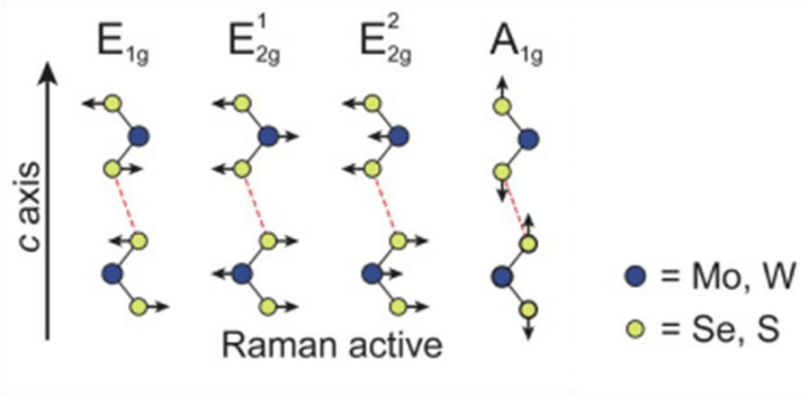

Figure 14. Schematic diagram of the Raman active modes[33] of WSe_2, WS_2, MoS_2 and $MoSe_2$.

We also observe both of the Raman modes (E^1_{2g} and A_{1g}) expected for monolayer MoS_2. The two characteristic peaks are identified at 385 cm^{-1}, which corresponds to the E^1_{2g} mode, and 406 cm^{-1}, which corresponds to its A_{1g} mode[34,35]. These numbers agree well with literature and since Raman spectra are fingerprints of the different materials, we can confidently deduce that the CVD method of synthesizing monolayer WSe_2 and MoS_2 is viable.

4.2.2 Optical Properties

Next, PL spectroscopy was carried out to obtain the PL spectra of the synthesized WSe_2 and MoS_2. Photoluminescence can be used to measure the quality and thickness of these monolayer TMDs. The PL spectrum of the as-grown monolayer WSe_2 , as shown in Figure 15a, exhibits a strong emission at 764 nm, which is in good agreement with other reports[15,22].

According to the Planck relation, the energy of the photons is related to the wavelength by

$$E = \frac{hc}{\lambda} \tag{3}$$

where E is the energy, h is the Planck's constant, c is the speed of light, and λ is the wavelength. Through simple calculations, the energy that corresponds to the wavelength of 764 nm is 1.63 eV, which coincides well with band gap of monolayer WSe_2[14,15].

Similarly, the PL spectrum of the as-grown monolayer MoS_2 , as shown in Figure 15b, also produces a very intense, single PL peak identified to be 666 nm. This wavelength corresponds to an energy band gap of 1.86 eV, which is indeed the band gap of monolayer MoS_2[16,23].

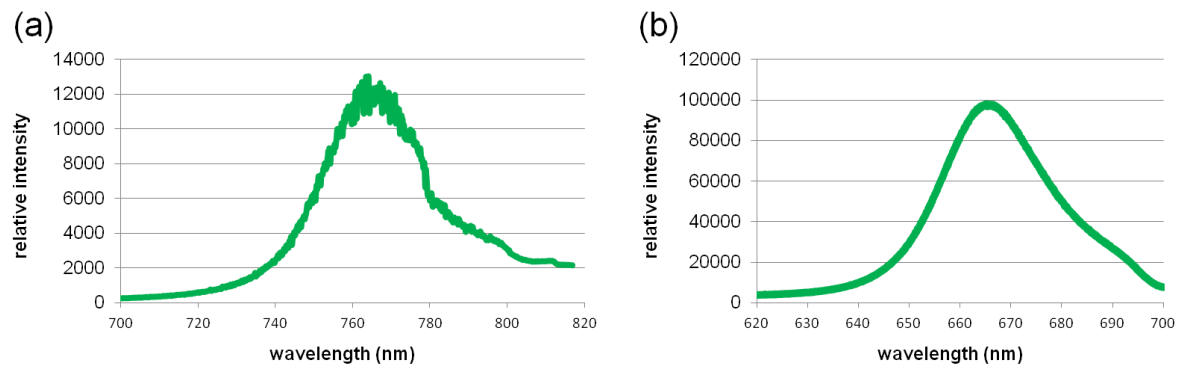

Figure 15. Photoluminescence spectra of as-grown monolayer (a) WSe_2 and (b) MoS_2.

The significant PL emission detected for both monolayer WSe_2 and MoS_2 is attributed to the direct band gap that monolayer TMDs possess and the PL peaks obtained for both materials correspond to their energy band gaps respectively. This further affirms that the as-grown WSe_2 and MoS_2 is indeed monolayer.

In addition to the PL spectra collected, the FM is also used to characterize the as-grown TMDs. Since the PL peak of WSe_2 is found to be 764 nm, which is in the near-infrared region of the electromagnetic spectrum, its fluorescence cannot be observed under the FM with the naked eye. Therefore, only FM images of MoS_2 are captured. Figure 16 shows the optical images of MoS_2 and their corresponding FM images, which show that the MoS_2 flakes exhibit a red fluorescence. This supports the fact that the synthesized MoS_2 flakes are monolayer, as the indirect band gap of a few-layered MoS_2 will quench the fluorescence[36].

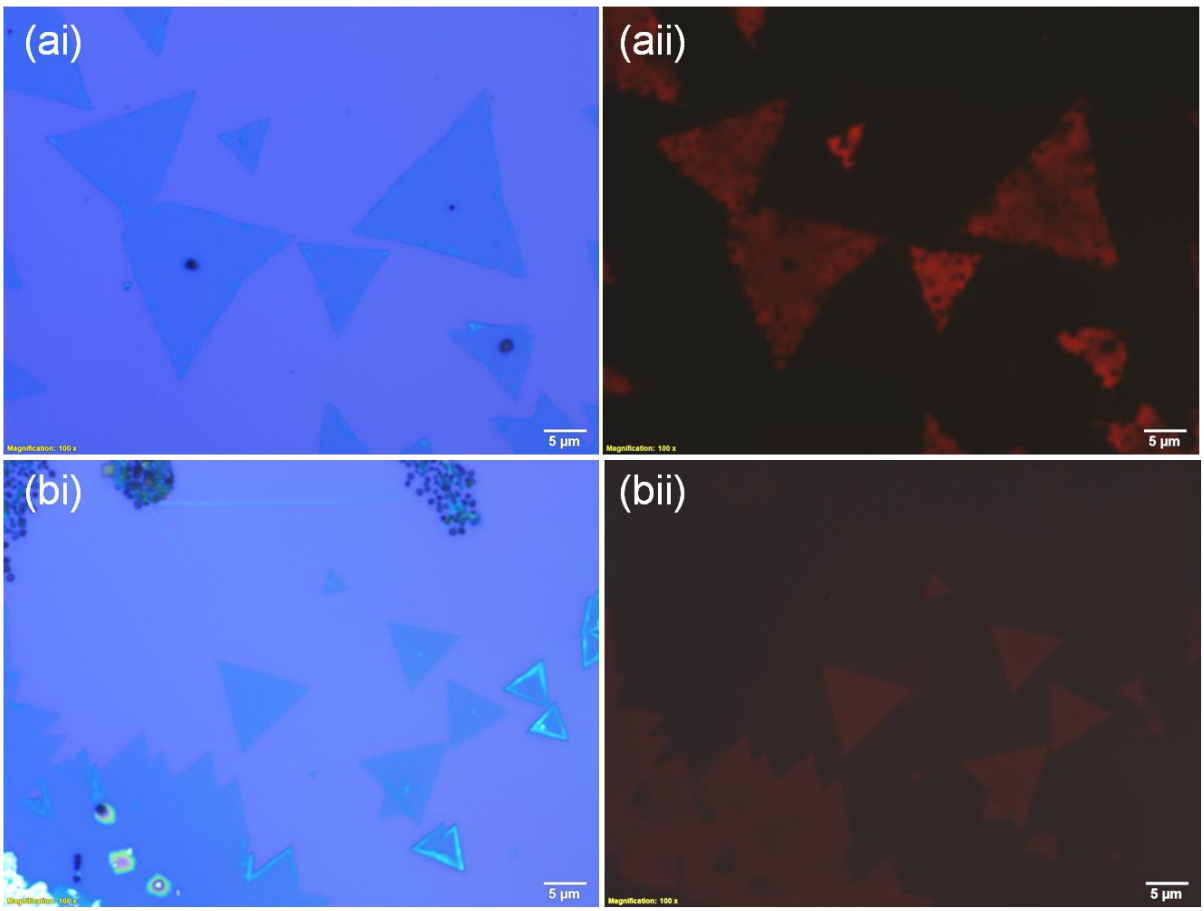

Figure 16. Optical image of (a) MoS_2 flakes synthesized without PTAS (i) under bright light and (ii) under yellow light. Optical image of (b) MoS_2 flakes synthesized with PTAS (i) under bright light and (ii) under yellow light.

The quenching of the fluorescence by few-layer MoS_2 can be observed from the FM images. The nucleation sites of the MoS_2 flakes, which appear as a black dot in the middle of the triangular flakes in Figure 16ai, as well as the thicker sides of some triangular flakes in Figure 16bi, fail to exhibit red fluorescence at their exact positions in the corresponding FM images. This is precisely due to the fact that few-layered MoS_2 no longer have direct band gaps and thus, they have different optical properties from monolayer MoS_2.

As mentioned in the previous section, two methods of monolayer MoS_2 synthesis are used in this project. It is experimentally observed that monolayer MoS_2 synthesized using the method that involves the addition of PTAS as a pre-synthesis step has a more uniform morphology. This can be seen when the samples are observed under the FM, using yellow light to incident on the as-grown monolayer MoS_2. By

comparing Figure 16aii and Figure 16bii, we can observe that MoS_2 synthesized with PTAS (Figure 16bii) displays an evenly distributed red fluorescence while MoS_2 synthesized without PTAS (Figure 16aii) does not have a uniformly distributed red fluorescence. Thus, it is deduced that the addition of PTAS before the synthesis of MoS_2 promotes greater uniformity of the monolayer growth. However, there seems to be a little compromise in the quality of MoS_2 due to the decrease in the intensity of the fluorescence. Unfortunately, due to time constraints and lack of reproducibility of the synthesis method without PTAS, there is a lack of data collected to adequately conclude about the quality of the MoS_2 synthesized.

4.2.3 AFM Imaging

The morphology and thickness of the synthesized material can be analyzed with the AFM. AFM images of as-grown monolayer WSe_2 and MoS_2 flakes are shown in Figure 17, appearing to be largely uniform in terms of its morphology. However, it is observed from the AFM image of WSe_2 in Figure 17a that there is a presence of some thick particles along the sides of the flake. This is speculated to be undesirable dirt particles due to prolonged storage of the as-grown WSe_2 under atmospheric conditions, as they were not observed under the optical microscope immediately after the synthesis process, but observed in this AFM image which was taken after a period of time. Figure 17b is a AFM image of a monolayer MoS_2 flake which was synthesized without the usage of PTAS. By making a comparison with the optical image of a similar monolayer MoS_2 flake in Figure 16ai, the spot observed near the middle of the MoS_2 flake in the AFM image is consistent with the appearance of a nucleation site near the middle of the MoS_2 flake observed in the optical image.

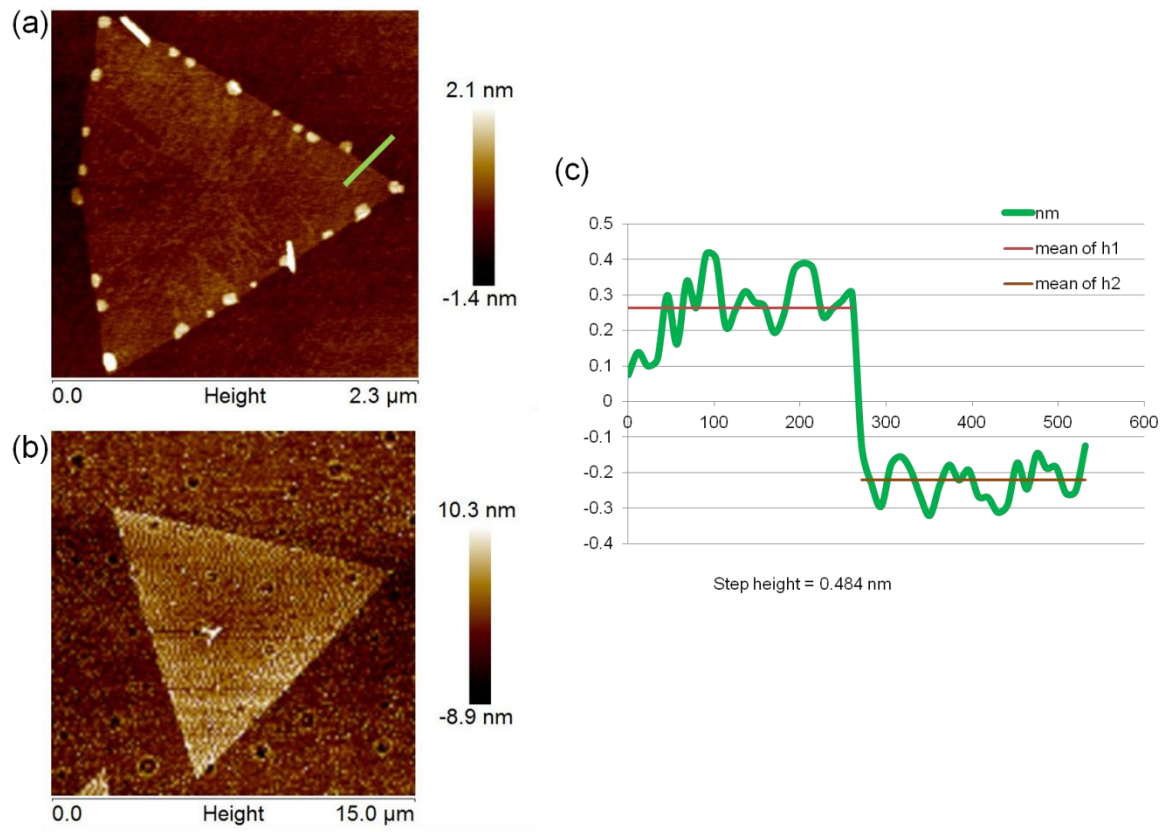

Figure 17. AFM images of as-grown monolayer (a) WSe_2 and (b) MoS_2 flakes. (c) Plotted height of a region on the monolayer WSe_2 flake, as indicated by green line in (a).

Information on the vertical distance across a section of the AFM image is obtained using the NanoScope Analysis software. The step height is found to be 0.484 nm, which is smaller than 0.65 nm, the expected height of monolayer TMDs[11]. It is suspected that there were some problems with the AFM, hence, this value may not be accurate. Subsequently, a fault was found in the calibration of the AFM machine when the AFM image of MoS_2 was taken, and due to time constraints, the AFM information collected regarding the thickness of the flake was inaccurate and unreliable. However, from the Raman spectra, PL spectra and FM images obtained for both as-grown WSe_2 and MoS_2, it can be concluded that monolayer TMDs are obtained through the synthesis processes.

4.2.4 Electrical Properties

To test the electrical properties of TMDs, devices were fabricated and tested. The following figure shows two I_d-V_d graphs of two of the devices fabricated in this project.

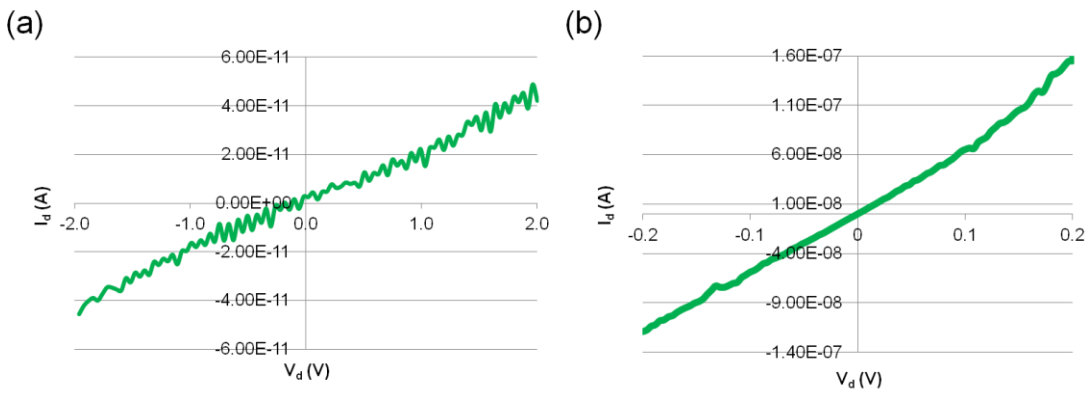

Figure 18. Graph of drain current I_d (A) against drain voltage V_d (V) of (a) a simple device fabricated with WS_2 on sapphire and (b) an ion gel FET device fabricated with WSe_2 on sapphire, with a gate voltage of -1.3 V applied.

The first is a simple device fabricated with a monolayer WS_2 flake on a sapphire substrate, having just two terminals, the source and the drain. The drain voltage V_d is varied from -0.2 V to 0.2 V and the current passing through the electrode I_d is recorded and plotted, as shown in Figure 18a. The second is an ion gel FET device fabricated with a region of monolayer WSe_2 on sapphire substrate, having three terminals, the source, the drain and the gate electrode. Figure 18b depicts the graph obtained when the drain voltage V_d is varied from -0.2 V to 0.2 V and a gate voltage V_g of -1.3 V is applied.

Both I_d-V_d curves are linear; Figure 18a has a coefficient of determination of r^2 = 0.992 while Figure 18b has a coefficient of determination of r^2 = 0.983. Since the I_d-V_d curves take on a linear shape, it can be deduced that the metal-semiconductor contact is Ohmic. This agrees with what is understood theoretically; to obtain an Ohmic metal-semiconductor contact for a p-type semiconductor, it requires the work function of the metal to be close to or larger than the band gap energy of the semiconductor, and for a n-type semiconductor, it has to be smaller[37]. In this project, Pd is used for the electrodes of WSe_2 devices and Cr is used for the electrodes of WS_2 devices. It is known that WSe_2 is a p-type semiconductor and WS_2 is a n-type semiconductor, and have work functions of 4.3 eV and 4.6 eV respectively[38], while the work function of Pd is 5.00 eV[39] and that of Cr is 4.40 eV[40]. Since $\Phi_{Pd} > \Phi_{WSe_2}$ and $\Phi_{Cr} < \Phi_{WS_2}$, the metal-semiconductor contacts are expected to be Ohmic.

Further analysis of the electrical properties of WSe_2, in comparison with its laser-modified counterpart, will be further explored in the sub-section on 'Comparison of Electrical Properties'.

4.3 Laser Modification of WSe_2 on Sapphire

After characterizing the as-grown WSe_2 flakes and verifying that they are indeed monolayer in thickness, the effect of laser modification of TMDs is investigated. Through systematic studies, it has been found that a laser power of approximately 100mW will not modify the morphology of WSe_2 flakes but is able to change its properties under ambient conditions. Using this knowledge, WSe_2 samples are subjected to laser modification; an area of 40 μm by 80 μm, with the presence of monolayer flakes within the area ensured, is subjected to the irradiation of laser light through the focused laser beam technique, with a laser power of approximately 100 mW and a velocity of 10 μm/s.

The Raman spectra of WSe_2 before and after laser modification are obtained and found to be identical. Since the width of a Raman peak is able to indicate the crystalline quality of the material, no change in the Raman peaks indicate that the crystalline quality of WSe_2 was not compromised upon laser modification. When observed under the AFM and FM, no change in morphology is observed.

Next, the PL spectra of the as-grown and laser-modified WSe_2 are obtained and shown in Figure 19. It can be observed that there is a very slight rightward shift in the peak after the material was laser-modified, and the peak becomes slightly broader. These observations might be attributed to the oxygen doping caused by laser modification.

It is proposed that the laser modification process under ambient conditions results in the introduction of oxygen into the material by encouraging it to fill up selenium vacancies in the WSe_2 lattice, simply using the atmosphere as a source of oxygen. This results in a slight change in the constituents of the material, which is reflected in the broadening of the PL spectra, as well as the slight shift in the peak position. However, this rightward shift is very minor, hence, the material is still largely monolayer WSe_2.

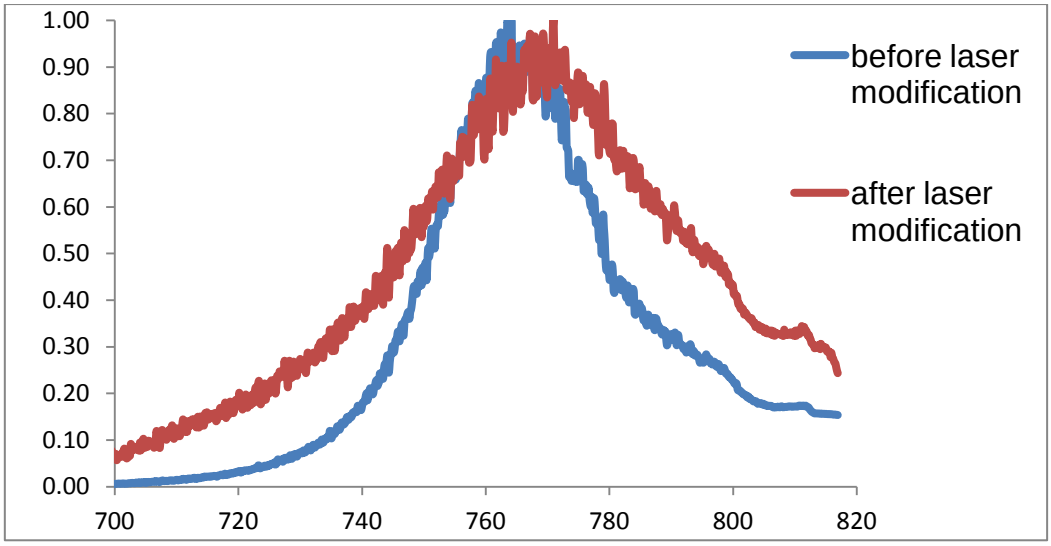

Figure 19. Normalized PL spectra of monolayer WSe_2 before and after laser modification.

As for the effect of laser modification on the electrical properties of TMDs, different FET devices are fabricated and tested. This will be further elaborated in the next sub-section.

4.4 Comparison of Electrical Properties

In this sub-section, the electrical properties of TMDs, WSe_2 in particular, will be analyzed and discussed, together with making comparisons with its laser-modified counterpart. In order to observe and compare the electrical properties of as-grown and laser-modified monolayer WSe_2, various ion gel FET devices are fabricated and tested. For example, a sample of successfully synthesized monolayer WSe_2 is used; after the deposition of electrodes (channel length L = 2 or 5μm, channel width W = 150 μm) on the sample on specific islands of monolayer WSe_2, a region on the sample is laser-modified before the ion gel solution is drop-casted, such that some devices use laser-modified islands as the channel material and others using the as-grown islands.

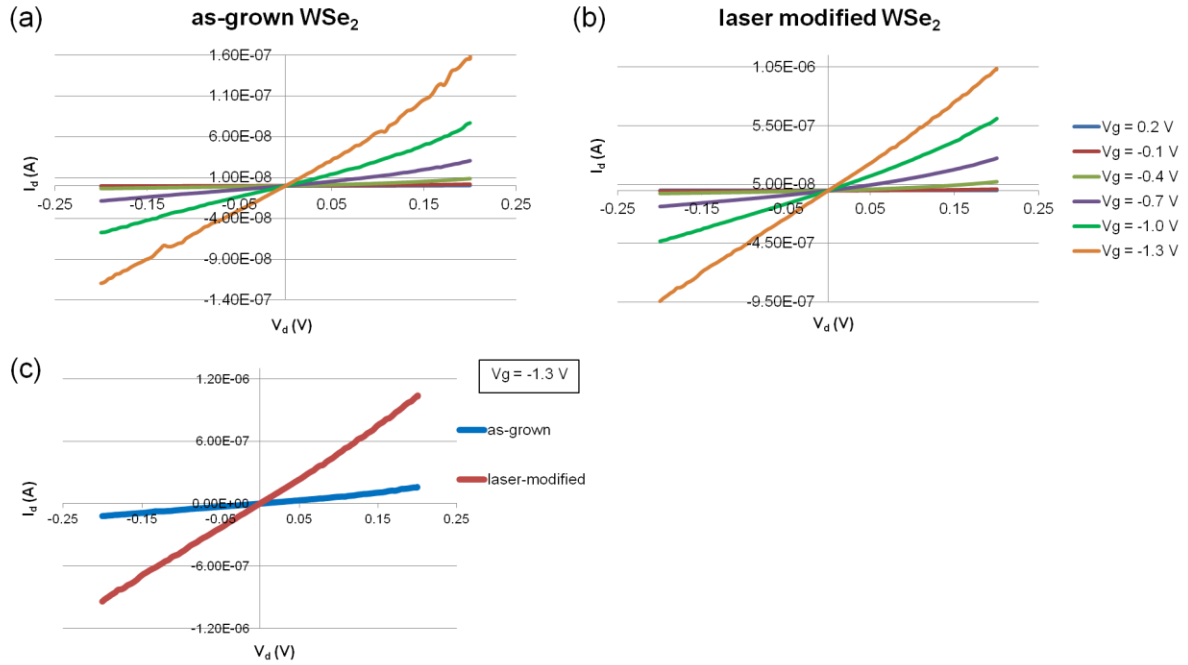

Figure 20. Multiple plots of drain current I_d (A) against drain voltage V_d (V) of an ion gel FET device fabricated with (a) as-grown WSe_2 on sapphire and (b) laser-modified WSe_2 on sapphire at varying gate voltages V_g. (c) Plot of current I_d (A) against drain voltage V_d (V) of as-grown device and laser-modified device when a gate voltage of -1.3 V applied.

When different gate voltages are applied to the FET device, it is observed that the I_d-V_d curve differs (Figures 20a and 20b). As the gate voltage V_g is decreased from 0.2 V to -1.3 V at intervals of 0.3 V, the I_d-V_d curves becomes steeper. This implies that

the electrical conductance, and hence the electrical conductivity, of the material increases as the applied V_g increases; in other words, the ability to conduct an electric current through the material increases. This is indeed the characteristic of FETs, which are voltage controlled devices, whereby the channel conductivity can be controlled by an external electric field by applying a gate voltage.

Upon understanding the behavior of FETs, we can now do a comparison between the device fabricated with as-grown monolayer WSe_2 and that which is fabricated with laser-modified monolayer WSe_2. The measured I_d-V_d plots indicate higher values of current for the device that is fabricated with laser-modified monolayer WSe_2. Evidently, Figure 20c shows that the gradient of the I_d-V_d curve of the laser-modified FET device is greater than that of the as-grown FET device. It is calculated that the conductance of the material increased by 6.5 times, showing an obvious improvement. Similar observations were made with the data obtained at other values of V_g. Even at V_g = 0.2 V, where the current measurements are low, a three-fold increase in its conductance is observed.

Next, the drain voltage V_d is fixed and I_d-V_g graphs are obtained, for both as-grown and laser-modified FET devices. Two examples are as shown in Figure 21; both sets of data are based on measurements made when the drain voltage V_d kept constant at 0.1 V. The graphs are also plotted in the logarithmic scale for the benefit of subsequent numerical calculations. Similarly, the I_d-V_g graphs indicate higher values of current for the device that is fabricated with laser-modified monolayer WSe_2.

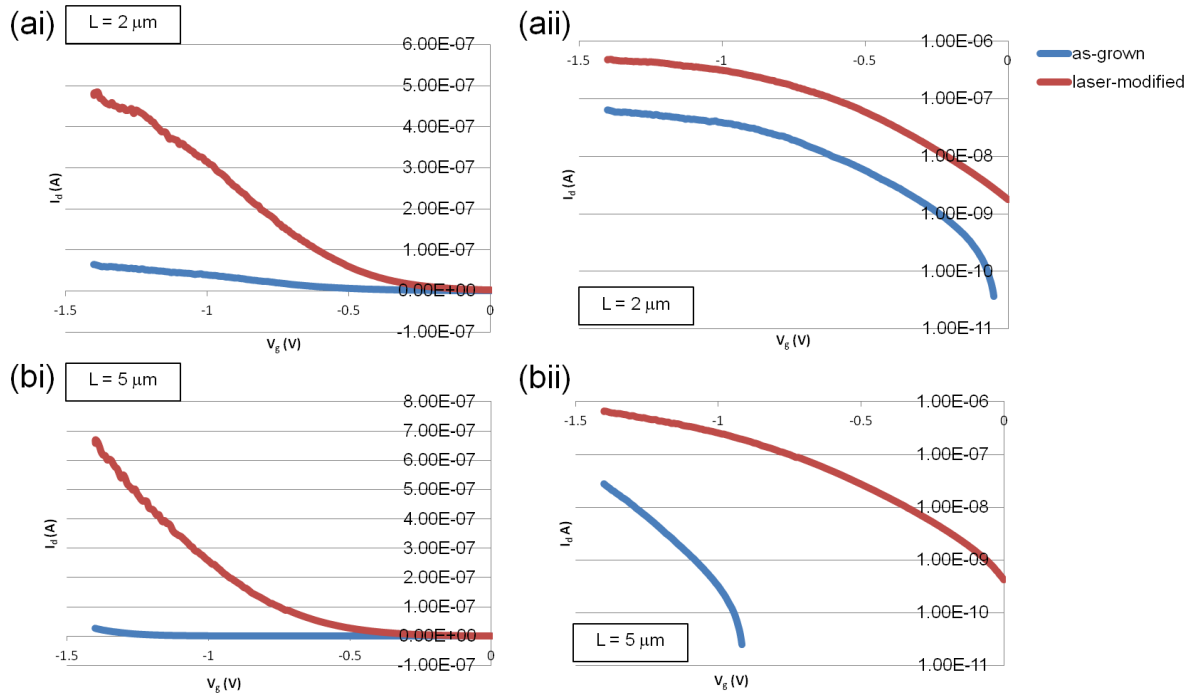

Figure 21. Graphs of drain current I_d (A) against gate voltage V_g (V) of an ion gel FET device fabricated with as-grown WSe_2 on sapphire and laser-modified WSe_2 on sapphire that has channel length L of (a) 2μm (i) in a linear scale and (ii) in a log scale, and (b) 5 μm (i) in a linear scale and (ii) in a log scale, with the drain voltage V_d kept constant at 0.1 V.

To have a more quantitative analysis, the field-effect mobility can be estimated from the following equation

$$\mu = \frac{L}{W C_0 V_d} \times \frac{\Delta I_d}{\Delta V_g} \qquad (4)$$

where μ is the field-effect mobility, L is the channel length, W is the channel width (150 μm), C_0 is the gate capacitance (10^{-6} F/cm^2), V_d is the drain voltage, I_d is the drain current and V_g is the gate voltage. Using Microsoft Excel, the gradients of the linear portion of the curves in Figure 21ai and 21bi are found and used to calculate the respective carrier mobilities for the hole transport of the two sets of data presented here. The calculated values are as shown in Table 2.

Channel Length L (μm)	Material of FET device	Mobility μ (cm^2/Vs)	Percentage Increase (%)
2	as-grown WSe_2	0.00855	648%
	laser-modified WSe_2	0.0639	
5	as-grown WSe_2	0.0541	650%
	laser-modified WSe_2	0.405	

Table 2. Table of two examples of calculated field-effect mobility and the percentage increase when comparing the as-grown value with the laser-modified value.

It is noticed that the mobility calculated is low compared to some of the previously reported mobility values of monolayer WSe_2, which could go as high as 100 cm^2/Vs. A possible reason for the low mobility could be that the electrical properties are highly sensitive to external conditions such as pressure, temperature or strain, which are not taken into account for[41]. All these factors could be better taken into account for through more detailed studies. Also, the ion gel used may not be the most ideal mixture to use as the gate electrode; other ion gels could be experimented with.

However, the results obtained through comparison of the carrier mobilities of the as-grown value with the laser-modified value in repeated measurements show a consistent six- to seven-fold increase. As proposed earlier, the laser modification process under ambient conditions results in the filling up of selenium vacancies in the WSe_2 lattice with oxygen atoms. Prior to the process, WSe_2 could be selenium-deficient due to its nature and high volatility. The presence of significant selenium vacancies can become electron traps, which thus limits the carrier mobility. When the selenium vacancies are occupied by oxygen atoms, these substitutional oxygen defects can create a better environment for carrier transport as they are electrically neutral impurities. This oxygen substitution of selenium vacancies may occur under ambient conditions with an abundant number of oxygen molecules in the air, but the reaction process will probably be very slow and the substitution cannot be easily controlled. Thus, the focused laser beam technique is useful as an efficient and effective treatment to facilitate the vacancy substitution.

Besides field-effect mobility, the carrier concentration n can also be estimated. The calculations of n are based on the equation

$$n = \frac{C_0 V_T}{e T} \quad (5)$$

where n is the carrier concentration, C_0 is the gate capacitance (10^{-6} F/cm^2), V_T is the threshold voltage, e is the electric charge and T is the thickness of the material (0.65 nm). Due to insufficient data collected, the threshold voltages and hence the carrier concentrations of the laser-modified FET devices cannot be calculated. The hole concentrations of the as-grown FET devices are found to be large, having values as high as 8.7×10^{15} cm^{-3}.

As the range of gate voltages V_g used is not large enough, the graphs in logarithmic scale do not possess the full shape of the expected I_d-V_g graphs, where the curve should taper off at both ends, limiting the calculations of on/off ratios as it requires the value of the current when the device saturates. Nevertheless, the on/off ratios can be estimated as a minimum value. The on/off ratios are found to be consistently of the magnitude of 10^3 for both as-grown and laser-modified devices, which is reasonable in comparison with previously reported values[22,42].

Results have consistently showed improvements in the electrical properties of ion gel FET devices fabricated from monolayer WSe_2. Hence, the focused laser beam technique is found to be a controllable way to improve these properties, and it is a step which can be easily adopted in the process of 2D TMDs electrical device fabrication.

5. Conclusion

5.1 Summary of Project

In this project, monolayer WSe_2 and MoS_2 flakes and islands were successfully synthesized using the chemical vapor deposition method. This was done by successfully optimizing the growth parameters, and it was found that both the MoS_2 and WSe_2 monolayers with high quality, regular shape and reasonable large sizes were obtained.

Upon successfully optimizing the growth parameters, both monolayer TMDs were characterized with the Fluorescence Microscope, Atomic Force Microscope, Photoluminescence Spectroscopy and Raman Spectroscopy. Following that, WSe_2 was laser-modified and characterized to observe the changes rendered to the material, and it is found to be largely identical to the as-grown monolayer WSe_2 in terms of its morphology, Raman properties and photoluminescence properties.

Subsequently, various devices were fabricated based on monolayer TMD flakes and islands, using the Electron Beam Lithography technique and thermal evaporation; at the same time, both as-grown and laser-modified monolayer WSe_2 islands were used as channel materials for the ion gel FET devices, so as to compare the differences between their electrical properties. Improvements are observed in the electrical properties of FET devices when the material is laser-modified, as seen from the consistent six- to seven-fold increase in the carrier mobilities for hole transport from the as-grown value to the laser-modified value. Also, the carrier concentration is found to be consistently within the range of 10^{14} to 10^{16} cm^{-3}, and the on/off ratios are found to be consistently of the magnitude of 10^3. Therefore, the laser modification technique is able to improve the electrical properties of TMDs, and is a promising method to be further explored to enhance TMD materials for the fabrication of devices.

5.2 Future Work

Due to time constraints, better understanding of PTAS and improved control over the amount of PTAS used was not explored enough in this project. Further studies could be conducted to obtain the optimum PTAS concentration, which will be useful in promoting the growth of monolayer TMDs. Besides the addition of PTAS, the regulation of the surface of the substrates through cleaning the substrates in a Piranha solution (H_2SO_4/H_2O_2 (3:1)) as a pre-synthesis process is a possible way to promote monolayer growth and could be further explored too[16].

As for the fabrication of ion gel FETs, other ion gels could be used to test their effectiveness as the gate electrode of WSe_2 ion gel FET devices, in order to identify the best ion gel solution to use and to optimize the enhancement of the electrical properties of WSe_2 FET devices. Also, the synthesis of other TMDs on sapphire substrates could be done to fabricate more ion gel FET devices for comparison between the different TMDs.

Besides comparing the electrical properties of as-grown and laser-modified TMDs, their optoelectronic properties can be analyzed as well. On top of fabricating FET devices, monolayer TMDs can also be used to fabricate optoelectronic devices such as photodetectors, light-emitting diodes and solar cells. Positive findings will further support the post-synthesis step of modifying as-grown TMDs using the focus laser beam technique for improved properties.

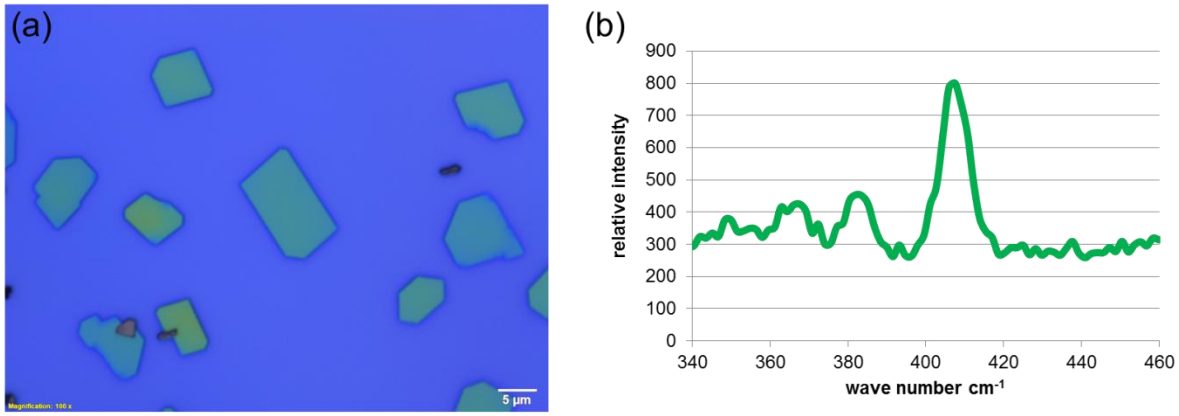

Figure 22. (a) Optical image of MoO_2 microplates. (b) Raman spectrum of one of the yellow microplates.

Lastly, through multiple runs of the chemical vapor deposition process for the optimization of growth parameters, an interesting finding was observed. It appears that when there is a higher concentration of PTAS, inferred from the thicker patterns left on the substrates after being heated dry, a different compound was discovered to have grown on the Si/SiO_2 substrates, as shown in Figure 22a. Upon obtaining a Raman spectrum of the compound (Figure 22b) and comparing it with literature, it was found to be MoO_2 flakes which are rhomboid in shape[43]. More experiments need to be conducted and these MoO2 microplates can be further analyzed and characterized.

References

1. Cooper, D.R., Anjou, B.D., Ghattamaneni, N., Harack, B., Hilke, M., Horth, A., Majlis, N., Massicotte, M., Vandsburger, L., Whiteway, E., Yu, V. (2011). Experimental review of graphene. *ISRN Condensed Matter Physics*, 2012, 1-56. doi: 10.5402/2012/501686

2. Bao, Q., Loh, K.P. (2012). Graphene photonics, plasmonics, and broadband optoelectronic devices. *ACS Nano*, (5), 3677-3694. doi: 10.1021/nn300989g

3. Geim, A.K., Novoselov, K.S. (2007). The rise of graphene. *Nature Materials*, 6, 183-191. doi:10.1038/nmat1849

4. Liu, L., Kumar, S.B., Ouyang, Y., Guo, J. (2011). Performance limits of monolayer transition metal dichalcogenide transistors (dissertation). doi: 10.1109/TED.2011.2159221

5. Peplow, M. (2013). The quest for supercarbon. *Nature*, 503, 327-329. doi: 10.1038/503327a

6. Wang, Q.H., Kalantar-Zadeh, K., Kis, A., Coleman, J.N., Strano, M.S. (2012). Electronics and optoelectronics of two-dimensional transition metal dichalocogenides. *Nature Nanotechnology*, 7, 699-712. doi: 10.1038/NNANO.2012.193

7. Hussain, A.M., Sevilla, G.A.T., Rader, K.R., Hussain, M.M. (2013). Chemical vapor deposition based tungsten disulfide (WS_2) thin film transistor (dissertation). doi: 10.1109/SIECPC.2013.6550981

8. Fang, H., Chuang, S., Chang, T.C., Takei, K., Takahashi, T., Javey, A. (2012). High-performance single layered WSe_2 p-FETs with chemically doped contacts. *Nano Letters*, 12, 3788-3792. doi: 10.1021/nl301702r

9. Shaw, J.C., Zhou, H., Chen, Y., Weiss, N.O., Liu, Y., Huang, Y., Duan, X. (2014). Chemical vapor deposition growth of monolayer $MoSe_2$ nanosheets. *Nano* Research, 1-9. doi: 10.1007/s12274-014-0147-z

10. Yu, L., Wang, H., Lee, Y.H., Ling, X., Fang, W., Hsu, A., Herring, P., Kong, J., Palacios, T. (2013). Electronics on MoS_2 and other 2D semiconductors. Retrieved from Massachusetts Institute of Technology, MTL annual research report 2013

website: http://www-mtl.mit.edu/wpmu/ar2013/electronics-on-mos2-and-other-2d-semiconductors/

11. Radisavljevic, B., Radenovic, A., Brivio, J., Giacometti, V., Kis, A. (2011). Single-layer MoS_2 transistors. *Nature Nanotechnology*, 6, 147-150. doi: 10.1038/NNANO.2010.279

12. Wilson, J.A., Yoffe, A.D. (1969). The transition metal dichalcogenides discussion and interpretation of the observed optical, electrical and structural properties. *Advances in Physics*, 18 (73), 193. doi: 10.1080/00018736900101307

13. Liang, W.Y. (1973). Optical anisotropy in layer compounds. *Journal of Physics: Solid State Physics*, 6, 551. doi: 10.1088/0022-3719/6/3/018

14. Baugher B.W.H., Churchill, H.O.H., Yang, Y., Jarillo-Herrero, P. (2014). Optoelectronic devices based on electrically tunable p-n diodes in a monolayer dichalcogenide. *Nature Nanotechnology*, 25, 1-6. doi: 10.1038/NNANO.2014.25

15. Elias, A.L., Perea-Lopez, N., Castro-Beltran, A., Berkdemir, A., Lv, R., Feng, S., Long, A.D., Hayashi, T., Kim, Y.A., Endo, M., Gutierrez, H..R., Pradhan, N.R., Balicas, L., Mallouk, T.E., Lopez-Urias, F., Terrones, H., Terrones, M. (2013). Controlled synthesis and transfer of large-area WS_2 sheets: from single layer to few layers. *ACS Nano*, 7 (6), 5235-5242.

16. Zande, A.M., Huang, P.Y., Chenet, D.A., Berkelbach, T.C., You, Y.M., Lee, G.H., Heinz, T.F., Reichman, D.R., Muller, D.A., Hone, J.C. (2013). Grain and grain boundaries in highly crystalline monolayer molybdenum disulphide. *Nature Materials*, 12, 554-561. doi: 10.1038/NMAT3633

17. Tongay, S., Zhou, J., Ataca, C., Lo, K., Matthews, T.S., Li, J., Grossman, J.C., Wu, J. (2012). Thermally driven crossover from indirect towards direct bandgap in 2D semiconductors: $MoSe_2$ versus MoS_2. *Nano Letters*, 12, 5576-5580. doi: 10.1021/nl302584w

18. Zhou, H., Wang, C., Shaw, J.C., Cheng, R., Chen, Y., Huang, X., Liu, Y., Weiss, N.O., Lin, Z., Huang, Y., Duan, X. (2015). Large area growth and electrical properties of p-type WSe_2 atomic layers. *Nano Letters*, 15, 709-713. doi: 10.1021/nl504256y

19. Ling, X., Lee, Y.H., Lin, Y., Fang, W., Yu, L., Dresselhaus, M.S., Kong, J. (2014). Role of the seeding promoter in MoS_2 growth by chemical vapor deposition. *Nano Letters*, 14, 464-472. doi: 10.1021/nl4033704

20. Lee, Y.H., Yu, L., Wang, H., Fang, W., Ling, X., Shi, Y., Lin, C.T., Huang, J.K., Chang, M.T., Chang, C.S., Dresselhaus, M., Palacios, T., Li, L.J., Kong, J. (2013). Synthesis and transfer of single-layer transition metal disulfides on diverse surfaces. *Nano Letters*, 13, 1852-1857. doi: 10.1021/nl400687n

21. Lee, Y.H., Zhang, X.Q., Zhang, W., Chang, M.T., Lin, C.T., Chang, K.D., Yu, Y.C., Wang, J.T.W., Chang, C.S., Li, L.J., Lin, T.W. (2012). Synthesis of large-area MoS2 atomic layers with chemical vapor deposition. *Advanced Materials*, 24, 2320-2325. doi: 10.1002/adma.201104798

22. Huang, J.K., Pu, J., Hsu, C.L., Chiu, M.H., Juang, Z.Y., Chang, Y.H., Chang, W.H., Iwasa, Y., Takenobu, T., Li, L.J. (2014). Large-area synthesis of highly crystalline WSe2 monolayers and device applications. *ACS Nano*, 8 (1), 923-930. doi: 10.1038/srep07293

23. Gomez, A.C., Barkelid, M., Goossens, A.M., Calado, V.E., Zant, H.S.J., Stelle, G.A. (2012). Laser thinning of MoS_2: on demand generation of a single-layer semiconductor. *Nano Letters*, 12, 3187-3192. doi: 10.1021/nl301164v

24. National University of Singapore. (2014). Scientists use simple, low cost laser technique to improve properties and functions of nanomaterials. Retrieved from Phys Org. Retrieved from http://phys.org/news/2014-07-scientists-simplelaser-technique-properties.html

25. Lu, J.P., Lim, X.D., Zheng, M.R., Subodh G. Mhaisalkar, Sow, C.H. (2012). Direct laser pruning of CdS_xSe_{1-x} nanobelts en route to a multicolored pattern with controlled functionalities. *ACS Nano*, *6* (9), 8298-8307.

26. Sze, S.M., Ng, K.K. (2007). Physics of Semiconductor devices (3rd ed.). Hoboken, New Jersey: John Wiley & Sons, Inc.

27. Woodford, C. (2015). *Transistors*. Retrieved from http://www.explainthatstuff.com/howtransistorswork.html.

28. *Ion Gel Gate Insulator in Field Effect Transistors.* (2015). *Retrieved* from http://license.umn.edu/technologies/z07062_ion-gel-gate-insulator-in-field-effect-transistors

29. Lee, J., Kakke, G., Cho, J.H., Zhu, X.Y., Lodge, T.P., Frisbie, C.D. (2009). Ion gel-gated polymer thin-film transistors: Operating mechanism and characterization of gate dielectric capacitance, switching speed, and stability. *J. Phys. Chem. C*, 113, 8972-8981. doi: 10.1021/jp901426e

30. Ho, J. C., Lee, J., Xia, Y., Kim, B., He, Y., Renn, M.J., Lodge, T.P., Frisbie, C.D. (2008). Printable ion-gel gate dielectrics for low-voltage polymer thin-film transistors on plastic. *Nature Materials*, 7, 900-906. doi: 10.1038/nmat2291

31. Chu, L., Schmidt, H., Pu, J., Wang, S., Ozyilmaz, B., Takenobu, T., Eda, G. (2014). Charge transport in ion-gated mono-, bi- and trilayer MoS^2 field effect transistors. *Scientific Reports*, 4, 7293

32. Mead, D.G., Irwin, J.C. (1977). Long Wavelength Optic Phonons in WSe2. *Can. J. Phys*, 55, 379-382.

33. Tonndorf, P., Schnidt, R., Bottger, P., Zhang, X., Borne, J., Liebig, A., Albrecht, M., Kloc, C., Gordon, O., Zahn, D.R.T., Vasconcellos, S.M., Bratschitsch, R. (2013). Photoluminescence emission and Raman response of monolayer MoS_2, $MoSe_2$ and WSe_2. *Optics Express*, 21 (4), 4908-4916.

34. Wu, S., Huang, C., Aivazian, G., Ross, J.S., Cobden, D.H., Xu, X. (2013). Vapor-solid growth of high optical quality MoS_2 monolayers with near-unity valley polarization. *ACS Nano*, 7 (3), 2768-2772. doi: 10.1021/nn4002038

35. Lee, C., Tan, H., Brus, L.E., Heinz, T.F., Hone, J., Ryu, S. (2010). Anomalous lattice vibrations of single- and few-layer MoS_2. *ACS Nano*, 4, 2695-2700.

36. Lv, R., Robinson, J.A., Schaak, R.E., Sun, D., Sun, Y., Mallouk, T.E., Terrones, M. (2014). Transition metal dichalcogenides and beyond: synthesis, properties, and applications of sngle- and few- layer nanosheets. *Accounts of chemical research*, 48, 56-64. doi: 10.1021/ar5002846

37. *Metal-semiconductor junction-ohmic contact*. (2015). Retrieved from http://www.doitpoms.ac.uk/tlplib/semiconductors/junction_ohmic.php.

38. Britnell, L., Ribeiro, R., Eckmann, A., Jalil, R., Belle, B., Mishchenko, A., Kim, Y.J., Gorbachev, R., Georgiou, T., Morozov, S. (2013). Strong light-matter interactions in heterostructures of atomically thin films. *Science*, 340, 1311-1314.

39. *Palladium*. (2015). Retrieved from http://www.chemistry-reference.com/q_elements.asp?Symbol=Pd.

40. *Chromium*. (2015). Retrieved from http://www.chemistry-reference.com/q_elements.asp?Symbol=Cr&language=en.

41. Roldan, R., Silva-Guillen, J.A., Lopez-Sancho, M.P., Guinea, F., Cappelluti, E., Ordejon, P. (2014). Electronic properties of single-layer and multilayer transition metal dichalcogenides MX_2 (M=Mo, W and X=S, Se). *Ann. Phys.*, 526 (9-10), 347-357. doi: 10.1002/andp.201400128

42. Chuang, H.J., Tan, X., Ghimire, N.J., Chamlagain, M.M.P.B., Cheng, M.M.C., Yan, J., Mandrus, D., Tomanek, D., Zhou, Z. (2014). High mobility p- and n-type field effect transistors contacted by highly doped graphene for low-resistance contacts. *Nano Letters*, 14 (6), 3594-3601. doi: 10.1021/nl501275p

43. Wang, X., Feng, H., Wu, Y., Jiao, L. (2013). Controlled synthesis of highly crystalline MoS2 flakes by chemical vapor deposition. *Journal of the American Chemical Society*, 135, 5304-5307. doi: 10.1021/ja4013485

"As we conquer peak after peak we see in front of us regions full of interest and beauty, but we do not see our goal, we do not see the horizon; in the distance tower still higher peaks, which will yield to those who ascend them still wider prospects, and deepen the feeling, the truth of which is emphasized by every advance in science, that 'Great are the Works of the Lord'."

-Sir Joseph J. Thomson, 1909